Directional Forces by Momentumless Excitation and Order-to-Order Transition in Peierls-Distorted Solids: The Case of GeTe

Nian-Ke Chen,[1] Xian-Bin Li,[1,*] Junhyeok Bang,[3] Xue-Peng Wang,[1] Dong Han,[4]
Damien West,[2] Shengbai Zhang,[1,2,†] and Hong-Bo Sun[1,‡]

[1]*State Key Laboratory of Integrated Optoelectronics, College of Electronic Science and Engineering, Jilin University, Changchun 130012, China*
[2]*Department of Physics, Applied Physics, and Astronomy, Rensselaer Polytechnic Institute, Troy, New York 12180, USA*
[3]*Spin Engineering Physics Team, Korea Basic Science Institute (KBSI), Daejeon 305-806, Republic of Korea*
[4]*State Key Laboratory of Luminescence and Applications, Changchun Institute of Optics, Fine Mechanics and Physics, Chinese Academy of Sciences, Changchun 130033, China*

Time-dependent density-functional theory molecular dynamics reveals an unexpected effect of optical excitation in the experimentally observed rhombohedral-to-cubic transition of GeTe. The excitation induces coherent forces along [001], which may be attributed to the unique energy landscape of Peierls-distorted solids. The forces drive the A_{1g} optical phonon mode in which Ge and Te move out of phase. Upon damping of the A_{1g} mode, phase transition takes place, which involves no atomic diffusion, defect formation, or the nucleation and growth of the cubic phase.

Ultrafast laser-induced phase transition plays important roles in a number of applications, such as micro- or nanoprocessing [1,2], device fabrication [3,4], and optical memory [5,6]. Understanding the underlying physics that governs the transition is the key to control the material's structure and thus the optimization of the device performance. By our count, there are four major types of phase transitions triggered by optical pulses. The first is melt quench, where the material is melt from its crystalline phase and then quenched to an amorphous phase [6,7]. The second is solid-state amorphization, where the crystal is directly transformed to its amorphous state without thermal melting [5,8–10]. The third is recrystallization, where a mild laser pulse supplies the required heat for a spontaneous crystallization [6,11]. The fourth is an order-to-order transition. For example, recently, an ultrafast order-to-order phase transition in GeTe under optical excitation was observed by time-resolved experiments with electron diffraction [12] and x-ray diffraction [13] techniques. This transition is excitation sustained and is hence transient.

The physical origin for the order-to-order transition is currently under debate. By femtosecond x-ray diffractions, Matsubara *et al.* [13] proposed a rattling model where, while the Te atoms maintain at their original positions, the Ge atoms rattle between six equivalent off-center positions of the rhombohedral (*r*) phase as a result of the excitation. The average effect of the rattling can be viewed as a transition to the higher-symmetry cubic (*c*) phase. On the other hand, based on an ultrafast electron diffraction technique, Hu *et al.* [12] suggested that the Te atoms are not fixed in their original positions, but exhibit a displacive

motion along the [001] direction. The motion is followed by a shear deformation of the lattice to result in the *c* phase. Time-resolved experiments offer important real-time information on the order-to-order transition. Kolobov *et al.* [14] performed a static first-principles calculation with fixed occupations to mimic optical excitation in *r*-GeTe. Based on the results, they proposed a third model in which the short and long bonds in *r*-GeTe are randomly distributed in space due to excitation, so the structure effectively becomes an averaged "pseudocubic" structure, while preserving locally the short and long bonds. These models differ owing to, among other things, the lack of a real-space atomic picture in real time. Time-dependent density-functional theory molecular dynamics (TDDFT-MD) is a technique that may overcome the problem, in particular, unveiling *real-time* interactions between electrons and lattice [15]. Recent examples demonstrated its applicability to phase change in a condensed matter [10,16].

In this Letter, we study dynamic electron-lattice coupling in GeTe by TDDFT-MD, which reveals the explicit role of electronic excitation on the rhombohedral-to-cubic (*r*-to-*c*) transition. Key in the finding is the excitation-induced directional (restoring) forces, which activate the A_{1g} phonon mode in the [001] direction. Atomic motions under the A_{1g} mode are along [001], coherent with a 180° phase shift; i.e., the Ge and Te atoms are always moving in the opposite directions. The creation of the coherent motion by the excitation destabilizes the Peierls distortion in the *r* phase to result in a displacive and diffusionless transition to the *c* phase. Note that the excitation-induced phase transition

takes place at temperatures substantially below the critical temperature within merely 1 ps.

The static density-functional theory (DFT) calculations are run in the VASP code [17,18] with projector augmented-wave (PAW) pseudopotential [19] and Perdew-Burke-Ernzerhof (PBE) exchange-correlation functional [20]. The cutoff energy for the plane wave expansion is 240 eV. The TDDFT-MD are run in the methodology developed by Meng and Kaxiras, as implemented in the SIESTA code [21], with norm-conserving Troullier-Martins pseudopotentials [22], PBE functional, and a NVE ensemble. The plane wave energy cutoff is 100 Ry and the local basis set with double-ζ polarized orbitals is employed. The coupling between atomic and electronic motions is governed by the Ehrenfest approximation [23], the time step is 0.024 fs, and the equilibrium state of *ab initio* MD at 300K is used as the input. In both DFT and TDDFT-MD, we use a 192-atom supercell for r-GeTe and the Γ point for Brillouin zone integration.

Figure 1 shows the atomic structure of r-GeTe, which consists of sixfold coordinated atoms in the form of an octahedron. Each atom has three p orbitals, p_x, p_y, and p_z, respectively, and each orbital can take up to two electrons. The Ge and Te atoms provide 2 and $4p$ electrons, respectively, to $3 + 3 = 6$ orbitals, which forms six bonds for each atom, as can be seen in Fig. 1(a). According to the electron counting model [24,25], each orbital is half filled [see also Fig. 1(a)]. The energy of the system can, however, be lowered by symmetry lowing, e.g., by a Peierls distortion [26] of the octahedra to result in (hierarchical) three short and three long bonds for each atom [see Fig. 1(b)] and a subsequent band gap opening. Figure 1(c) shows the supercell used in the simulation along with its primitive unit cell.

Figure 2(a) shows the partial density of states for r-GeTe and its occupation upon a 5% excitation of valence electrons. We choose 5% here, as it corresponds to a 13 mJ/cm^2 fluence that can be readily obtained by laser experiment [5,27,28]. In fact, the results for the excitations
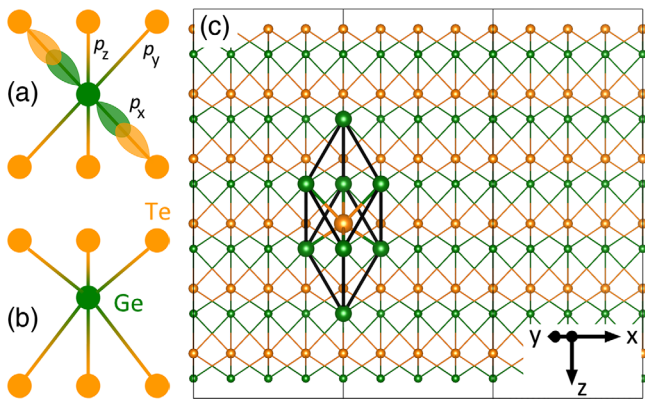
from 4.5% to 6% is quantitatively the same in our calculations. Figure 2(b) shows schematic real-space potential energy surfaces (PESs) of a Ge atom along [001]. Since the motion of the Ge atom is relative to the neighboring Te atoms, the same PESs apply to the Te atom as well. In the (r phase) ground state, there are two energy minima representing two equivalent Ge positions. In the excited state, however, the system restores the cubic symmetry for which there is only one energy minimum. Because of this qualitative change in the PES upon excitation (see the vertical dashed line), restoring force on the atom alone [001] is generated [see the arrow in Fig. 2(b)].

Although the calculation employs a supercell with 96 GeTe molecules, the forces generated on these atoms are all coherent, as can be seen by the direction and magnitude of the arrows in Fig. 2(c). It implies that the directional forces are not a result of a constrained calculation using a too small supercell, but rather it represents a real physical effect, namely, the symmetry of the r phase. One can readily see the symmetry after the excitation by examining the real-space charge density difference (CDD) [also plotted in Fig. 2(c)]. Here, CDD is defined as ρ (excited state)–ρ (ground state). It shows that, after the excitation, electrons are accumulated around the Ge atoms, at the expense of electrons around the Te atoms. However, only
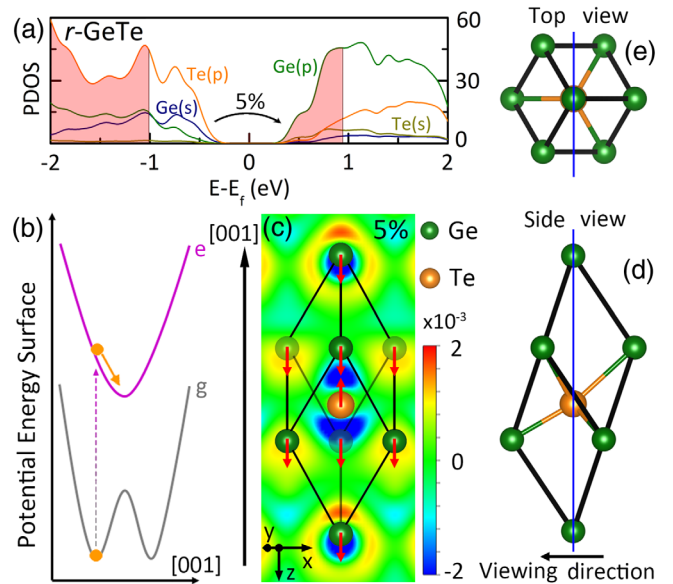

FIG. 2. (a) Partial density of states (PDOS). Shaded areas indicate a rough estimate on what would be the occupations of the states upon a 5% excitation. (b) Potential energy surfaces (PESs). Gray line is the ground state, whereas the purple line is the excited state. (c) Atomic forces (red arrows) due to excitation. Graded green color indicates the positions of the Ge atoms (solid is in front and faint is in the back). Charge density difference between ground and excitation states is also shown on a plane cutting through the center of the primitive unit cell, as shown by the solid blue line in (d) and (e). The unit of CDD is e/a_0^3, where a_0 is the Bohr radius.

FIG. 1. Atomic motifs of (a) c-GeTe and (b) r-GeTe. (c) The supercell used in simulation. The rhombohedral primitive cell is highlighted by larger balls.

the symmetry along the z axis ($=$[001] direction of r-GeTe) is broken, and that in the x-y plane remains intact. In Ge-Sb-Te alloys, in contrast, due to the disorder of the vacancies on the cation lattice, the degree of the coherence is expected to be reduced.

Next, we discuss the results obtained by TDDFT-MD simulations. Figure 3 depicts the real-time force, bond length, bond angle, and ionic temperature (further explained in Note 1 of the Supplemental Material [29]) in a TDDFT-MD simulation with a 5% excitation in GeTe. As expected, forces in Fig. 3(a) are highly directional throughout the simulation: in particular, forces along the z axis are strongest at the onset but gradually decrease with time, and at 1.1 ps, they almost all approach zero. In contrast and with no exception, forces in the other directions can be neglected during the simulation. Figures 3(b) and 3(c) capture the structural responses to the forces, where the long (and short) bond lengths and the high (and low) bond angles of the r phase at the beginning give way to equal bond lengths and bond angles at the end of the simulation. In other words, r-GeTe undergoes a transition to c-GeTe.

To be certain that the effects in Fig. 3 are mainly due to excitation, we performed *ab initio* MD for 1.2 ps without the excitation. We found essentially no changes in the quantities plotted in Fig. 3 up to 700 K; see Note 2 and Fig. S1 of the Supplemental Material [29]. With the excitation, phase transition happens at 500 K, which is noticeably lower than the melting point (T_m) of GeTe [see Fig. 3(d)] [30]. It is also significantly lower than the critical temperature for the ferroelectric transition of r-GeTe [31]. Although the transient ionic temperature at 75 fs can reach 650 K, further analyses in Note 3 and Fig. S2 of the Supplemental Material [29] demonstrate that the nominally high temperature has nothing to do with thermal motion, but is merely a result of the correlated out-of-plane motion of the atoms due to optical excitation.

Figure 4 shows the time evolution of bond-length probability density distribution $f(x)$ during phase transition. Here, the integrated probability

$$P = \int_{-\infty}^{+\infty} f(x)dx = 1.$$

At the ground state, the bond lengths are hierarchical. After excitation, the long and short bonds quickly become equal length. Gaussian fitting in Fig. 4 quantifies the amount of remaining short and long bonds that decrease with time and
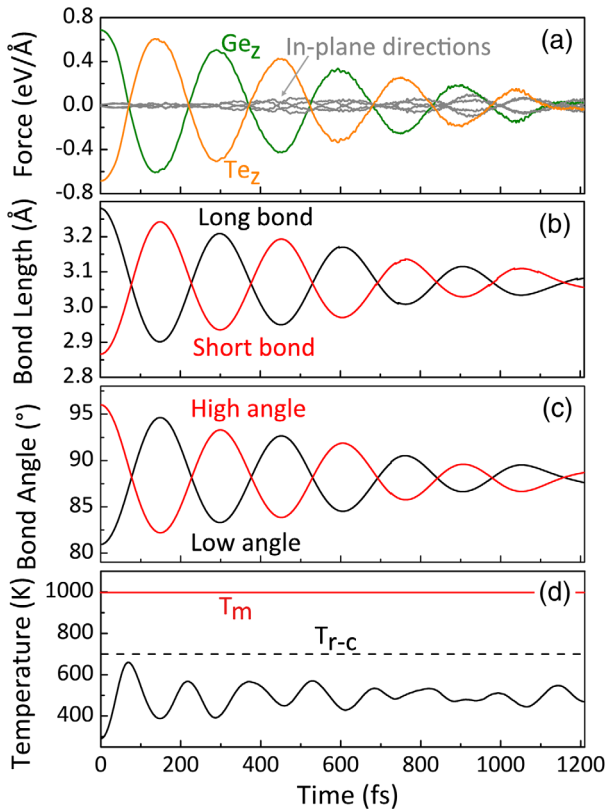

FIG. 3. Time evolution of average (a) force, (b) bond length, and (c) angle and (d) ionic temperature of GeTe with a 5% excitation. Red solid and black dashed lines in (d) indicate, respectively, the melting point (T_m) and Curie temperature (T_{r-c}) for ferroelectric transition taken from literature [30,31].
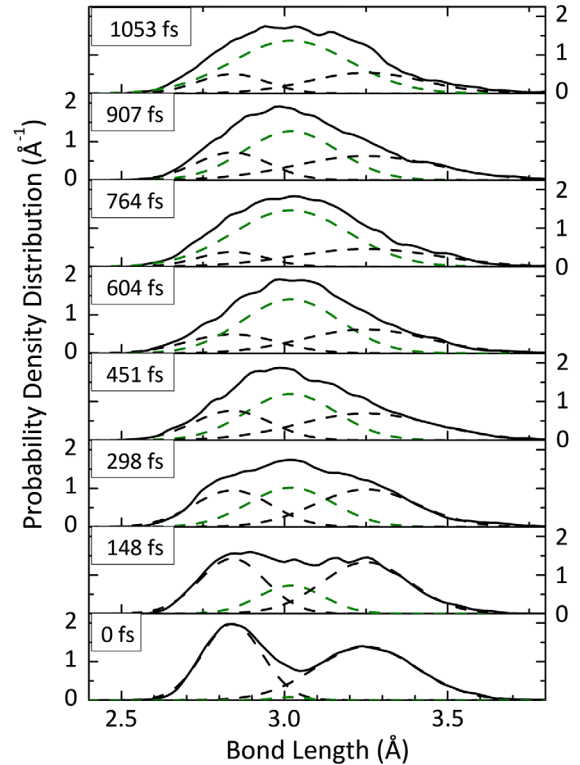

FIG. 4. Time evolution of bond-length probability density distribution after excitation. Time taken for the plot corresponds to peaks and valleys in Fig. 3(b) at which the differences in bond lengths are largest. Dashed lines are Gaussian fitting with peak positions at 2.84, 3.02, and 3.25 Å, respectively. It appears that the central green line will further grow at the expense of others for $t > 1053$ fs.

become insignificant at $t = 604$ fs. The integrated probability for short and long bonds is roughly 99% in the beginning of the simulation but less than 37% in the end. It supports the notion that a majority of the short or long bonds has been converted to bonds with equal lengths [12]. Hence, the transition is truly a r-to-c transition, rather than a "pseudo" one due to some sort of averaging effect. This is qualitatively different from the thermally induced r-to-c transition, as the latter is due to a lack of the coherent and directional forces and hence can only be attributed to the randomization of long and short bonds [32,33].

Usually, atomic motion during laser-matter interaction is difficult to control due to the lack of momentum of the photons. As such, light can excite almost any atomic vibration at the center of the Brillouin zone, leading to a structural disorder and/or amorphization. Here, however, although the incident photons remain momentumless, the unique energy landscape in Fig. 2(b) makes an important difference; namely, before the excitation, there are two energy minima along [001] that are significantly different from the single minimum after the excitation. As such, all the atoms after the excitation are forced to move in the [001] direction collectively, as well as coherently. The coherency arises because the Ge and Te atoms must move in the opposite directions to preserve a net-zero momentum. This initial motion couples to lattice vibrations that can sustain a back-and-forth flipping of the long and short bonds.

The A_{1g} optical phonon mode satisfies such a constraint and, as a matter of fact, is in resonance with the initial excitation. No other phonon modes get excited by the optical excitation, as revealed by our TDDFT-MD simulation. See, for example, the evolution of atomic forces and bond lengths in Fig. 3, which is indicative of the flip-flop of the long and short bonds. Direct evidence of such a motion
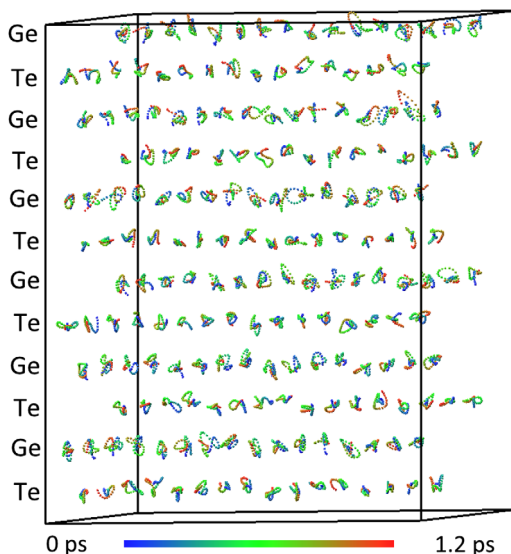
is given in Note 4 and Fig. S3 of the Supplemental Material [29], where we trace the atomic motion in real space over a half vibration period.

We can also trace the A_{1g}-mode frequency using Fig. 3(b) to original 3.33 THz. This value is about 12% less than the 3.8 THz for the A_{1g} mode in the ground state [34]. The redshift of the A_{1g}-mode frequency agrees with experiments of 8% (redshift) at a similar fluence [34]. The A_{1g} mode couples to other phonon modes during the TDDFT-MD simulation, which leads to the damping of its magnitude and eventually to the r-to-c transition in GeTe. The transition is diffusionless, as evidenced by Fig. 5, which records the trajectories of all the atoms. Throughout the MD simulation, there is no defect formation, no nucleation and growth, and no single diffusion across any atomic site.

In conclusion, TDDFT-MD simulation reveals the salient physics of optical excitation on order-to-order transition. Although the photons are momentumless, by exciting the system from a double-minima state to a single-minimum state, they enable a coherent and collective motion of the atoms, which couples strongly to the A_{1g} optical phonon mode. While the current Letter focuses on phase transition in GeTe, it is not an isolated case. In fact, all ferroelectric solids, to which GeTe belongs to, or more broadly speaking, all solids with Peierls distortion have the characteristic energy landscape in Fig. 2(b). As a matter of fact, in Peierls-distorted Bi, Sb, Te, and Ti_2O_3, laser selective excitation of the A_{1g} mode has been observed [35]. It is thus reasonable to believe that our phase transition mechanism may apply to many of them and as such, our finding opens a new direction in the search for ultrafast ordered phase change materials for electronic, optoelectronic, and energy applications.

N.-K. C. and X.-B. L. are contributed equally to this work.

FIG. 5. Trajectories of atomic motion in the time frame from 0 to 1.2 ps in the TDDFT-MD simulation with a 5% excitation.

*Corresponding author:
lixianbin@jlu.edu.cn
†Corresponding author:
zhangs9@rpi.edu
‡Corresponding author:
hbsun@jlu.edu.cn

[1] S. Kawata, H.-B. Sun, T. Tanaka, and K. Takada, Nature (London) **412**, 697 (2001).

[2] K. Sugioka and Y. Cheng, Light Sci. Appl. **3**, e149 (2014).

[3] Y. L. Sun, Q. Li, S. M. Sun, J. C. Huang, B. Y. Zheng, Q. D. Chen, Z. Z. Shao, and H. B. Sun, Nat. Commun. **6**, 8612 (2015).

[4] D. Yin, J. Feng, R. Ma, Y. F. Liu, Y. L. Zhang, X. L. Zhang, Y. G. Bi, Q. D. Chen, and H. B. Sun, Nat. Commun. **7**, 11573 (2016).

[5] X.-B. Li, X. Q. Liu, X. Liu, D. Han, Z. Zhang, X. D. Han, H.-B. Sun, and S. B. Zhang, Phys. Rev. Lett. **107**, 015501 (2011).

[6] M. Wuttig and N. Yamada, Nat. Mater. **6**, 824 (2007).

[7] A. V. Kolobov, P. Fons, A. I. Frenkel, A. L. Ankudinov, J. Tominaga, and T. Uruga, Nat. Mater. **3**, 703 (2004).

[8] M. Konishi, H. Santo, Y. Hongo, K. Tajima, M. Hosoi, and T. Saiki, Appl. Opt. **49**, 3470 (2010).

[9] S. K. Sundaram and E. Mazur, Nat. Mater. **1**, 217 (2002).

[10] C. Lian, S. B. Zhang, and S. Meng, Phys. Rev. B **94**, 184310 (2016).

[11] J. Hegedus and S. R. Elliott, Nat. Mater. **7**, 399 (2008).

[12] J. Hu, G. M. Vanacore, Z. Yang, X. Miao, and A. H. Zewail, ACS Nano **9**, 6728 (2015).

[13] E. Matsubara, S. Okada, T. Ichitsubo, T. Kawaguchi, A. Hirata, P. F. Guan, K. Tokuda, K. Tanimura, T. Matsunaga, M. W. Chen, and N. Yamada, Phys. Rev. Lett. **117**, 135501 (2016).

[14] A. V. Kolobov, P. Fons, J. Tominaga, and M. Hase, J. Phys. Chem. C **118**, 10248 (2014).

[15] E. Runge and E. K. U. Gross, Phys. Rev. Lett. **52**, 997 (1984).

[16] J. Bang, Y. Y. Sun, X. Q. Liu, F. Gao, and S. B. Zhang, Phys. Rev. Lett. **117**, 126402 (2016).

[17] G. Kresse and J. Furthmuller, Comput. Mater. Sci. **6**, 15 (1996).

[18] G. Kresse and J. Furthmuller, Phys. Rev. B **54**, 11169 (1996).

[19] G. Kresse and D. Joubert, Phys. Rev. B **59**, 1758 (1999).

[20] J. P. Perdew, K. Burke, and M. Ernzerhof, Phys. Rev. Lett. **78**, 1396 (1997).

[21] S. Meng and E. Kaxiras, J. Chem. Phys. **129**, 054110 (2008).

[22] N. Troullier and J. L. Martins, Phys. Rev. B **43**, 1993 (1991).

[23] J. L. Alonso, X. Andrade, P. Echenique, F. Falceto, D. Prada-Gracia, and A. Rubio, Phys. Rev. Lett. **101**, 096403 (2008).

[24] M. C. Lucking, J. Bang, H. Terrones, Y.-Y. Sun, and S. Zhang, Chem. Mater. **27**, 3326 (2015).

[25] M. D. Pashley, Phys. Rev. B **40**, 10481 (1989).

[26] R. Peierls and A. O. Barut, Am. J. Phys. **60**, 957 (1992).

[27] M. Cardona and D. L. Greenaway, Phys. Rev. **133**, A1685 (1964).

[28] J. E. Lewis, Phys. Status Solidi B **59**, 367 (1973).

[29] See Supplemental Material at http://link.aps.org/supplemental/10.1103/PhysRevLett.120.185701 for the explanatory note of ionic temperature in TDDFT-MD; Fig. S1: comparison of the time evolutions of temperature profile, average force and bond length of GeTe between ground-state MD (700 K) and excited-state MD; Fig. S2: the analyses on kinetic energy, momentum, and thermal temperature to show that thermal effect is not the reason for the ultrafast r-c transition in our simulation; Fig. S3: snapshots of TDDFT-MD simulation of 5%-excited GeTe at $t = 0$ and 148 fs to display the flipping of the short and long bonds during the excitation.

[30] K. L. Chopra and S. K. Bahl, J. Appl. Phys. **40**, 4171 (1969).

[31] G. S. Pawley, W. Cochran, R. A. Cowley, and G. Dolling, Phys. Rev. Lett. **17**, 753 (1966).

[32] P. Fons, A. V. Kolobov, M. Krbal, J. Tominaga, K. S. Andrikopoulos, S. N. Yannopoulos, G. A. Voyiatzis, and T. Uruga, Phys. Rev. B **82**, 155209 (2010).

[33] T. Matsunaga, P. Fons, A. V. Kolobov, J. Tominaga, and N. Yamada, Appl. Phys. Lett. **99**, 231907 (2011).

[34] M. Hase, K. Mizoguchi, and S. Nakashima, J. Lumin. **87–89**, 836 (2000).

[35] H. J. Zeiger, J. Vidal, T. K. Cheng, E. P. Ippen, G. Dresselhaus, and M. S. Dresselhaus, Phys. Rev. B **45**, 768 (1992).